Acta Crystallographica Section D
Biological Crystallography
ISSN 0907-4449

Intermonomer interactions in dimer of bovine heart cytochrome *c* oxidase

Soo Jae Lee,[a] Eiki Yamashita,[a] Toshio Abe,[b] Yoshihisa Fukumoto,[b] Tomitake Tsukihara,[a] Kyoko Shinzawa-Itoh,[c] Hidehumi Ueda[d] and Shinya Yoshikawa[c]*

[a]Institute for Protein Research, Osaka University, 3-2 Yamada-oka, Suita 565-0871, Japan, [b]Faculty of Engineering, Tottori University, Tottori 680-0945, Japan, [c]Department of Life Science, Himeji Institute of Technology and CREST, Japan Science and Technology Corporation (JST), Kamigohri Akoh, Hyogo 678-1297, Japan, and [d]Department of Applied Chemistry, Himeji Institute of Technology, 2167 Shosha Himeji, Hyogo 671-2201, Japan

Correspondence e-mail: yoshi@sci.himeji-tech.ac.jp

Received 11 December 2000
Accepted 30 March 2001

The X-ray structure of bovine heart cytochrome *c* oxidase solved for orthorhombic crystals showed a dimeric structure stabilized by four subunit–subunit contacts, namely, subunit Vb–subunit Vb on the matrix side, subunit I–subunit VIa, subunit VIa–subunit I in the transmembrane region and subunit VIb–subunit VIb on the intermembrane side. The same intermonomer contacts as in the orthorhombic crystals were observed in both hexagonal and tetragonal crystals, the X-ray structures of which were determined by the molecular-replacement method. These results suggest that the dimeric structure also exists under physiological conditions. These contacts, especially the subunit IVa–subunit I contact, in which the N-terminal portion of subunit IVa is placed on the surface of subunit I near the dioxygen-reduction site, indicate that the function of the bovine heart enzyme is likely to be controlled by perturbation of the monomer–monomer association.

1. Introduction

Bovine heart cytochrome *c* oxidase is a multisubunit membrane protein in the mitochondorial respiratory chain that is involved in dioxygen reduction coupled with proton translocation across the mitochondrial membrane (Ferguson-Miller & Babcock, 1996). The crystal and molecular structures of the enzyme have been determined at 2.8 Å resolution (Tsukihara *et al.*, 1995, 1996; Tomizaki *et al.*, 1999) and refined to 2.3 Å resolution (Yoshikawa *et al.*, 1998) in our laboratories. The X-ray structure has showed 13 different subunits as in Fig. 1 (three mitochondrially coded subunits and ten nuclear-coded subunits).

It has been proposed that purified bovine heart cytochrome *c* oxidase was in either a monomeric or dimeric state depending on the coexisting detergent species and/or phospholipids (Finel & Wikström, 1986; Capaldi & Zhang, 1986; Hakvoort *et al.*, 1987; Estey & Prochaska, 1993). However, the nature and the physiological significance of the dimerization is still controversial.

This paper presents the detailed dimeric structure of bovine heart cytochrome *c* oxidase stabilized by nuclear-coded subunits. The dimeric state was not influenced by significant changes in crystal packing.

2. Experimental and structural determination

2.1. Crystallization and intensity data acquisition

Bovine heart cytochrome *c* oxidase can be crystallized in hexagonal, tetragonal and orthorhombic forms under different crystallization conditions, as described previously

© 2001 International Union of Crystallography
Printed in Denmark – all rights reserved

(Yoshikawa *et al.*, 1991, 1992; Shinzawa-Itoh *et al.*, 1992, 1995). By soaking in such heavy-atom reagents as tetrakis(acetoxymercuri)methane, the tetragonal crystal could be transformed into a different phase of the same tetragonal system. The intensity data for these crystals were collected at the Photon Factory, Institute for High Energy Physics, Tsukuba, Japan by the oscillation method, using a Weissenberg camera equipped with an imaging plate designed by Sakabe (1983) for macromolecules with large unit-cell dimensions. Diffraction images were processed using the program *WEIS* (Higashi, 1989) and observed reflections were scaled by the method of Hamilton *et al.* (1965).

2.2. Crystal structure determination

The molecular-replacement method (Rossmann & Blow, 1962) was used for structure determination of the hexagonal and tetragonal crystals. The initial phases of the hexagonal crystal were obtained by locating the 13 subunit monomeric structures of the orthorhombic form determined at 2.8 Å resolution (Tsukihara *et al.*, 1995, 1996; Tomizaki *et al.*, 1999). The crystal structure was refined by the rigid-body refinement method using a constrained monomeric structure in an asymmetric unit. The program *X-PLOR* v.3.1 (Brünger *et al.*, 1987) was employed for the crystal structure determination of the hexagonal crystal.

Table 1
Intensity data collection for hexagonal and tetragonal crystals.

		Tetragonal	
	Hexagonal	I	II
Experimental conditions			
Wavelength (Å)	1.48	1.48	1.00
Exposure time (s)	84.0	84.0	84.0
Oscillation range (°)	4.2	5.5	4.2
Camera radius (mm)	429.8	429.8	573.0
Crystal data			
Space group	$P62$	$I4_122$	$I4_122$
Unit-cell parameters			
$a = b$ (Å)	208.7 (6)	273.1 (6)	253.2 (4)
c (Å)	282.3 (12)	170.9 (6)	507.1 (6)
$\alpha = \beta$ (°)	90	90	90
γ (°)	120	90	90
Z†	6	8	24
V_M‡ (Å^3 Da^{-1})	8.61	7.74	6.76
Solvent content‡ (%)	85.7	84.1	81.8
Intensity data			
Resolution (Å)	100.0–7.0	70.0–15.0	100.0–6.0
Reflections [$F > 2\sigma(F)$]			
No. observed	32758	3236	15096
No. independent	7026	531	9511
R_{merge}§	0.095	0.046	0.095

† Z is the number of enzyme complexes consisting of 13 subunits in the unit cell. ‡ V_M and solvent content were determined according to Matthews (1968). § $R_{merge} = \sum\sum|\langle I(hkl)\rangle - I_i(hkl)|/\sum\sum I_i(hkl)$.

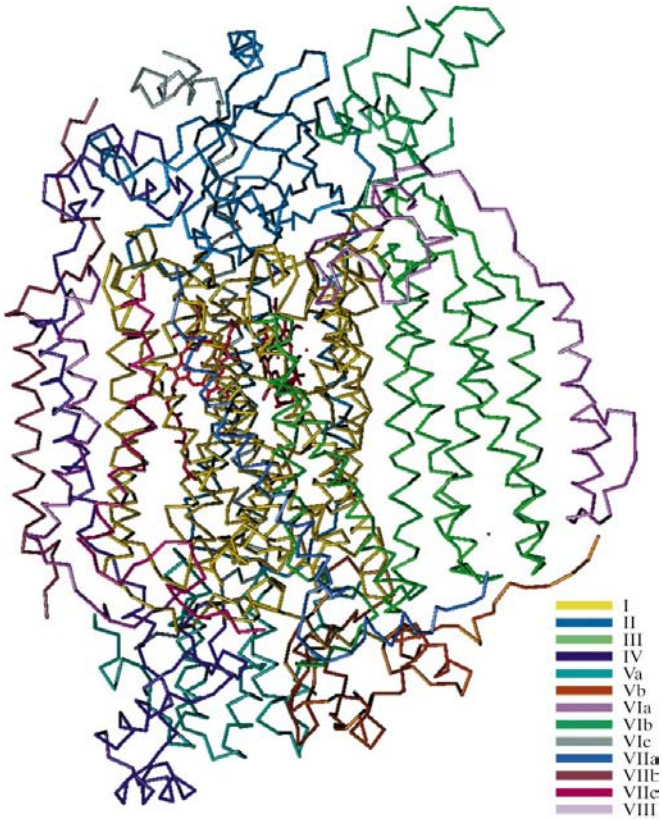

Figure 1
13 subunit structures of bovine heart cytochrome *c* oxidase are depicted by C^{α} trace: view of the transmembrane surface. The intermembrane side is at the top. Each subunit is shown in a different colour. Polypeptides in the transmembrane region fold in α-helices. Subunits I, II and III encoded by mitochondrial genes form a core, while the other subunits surrounding the core subunits are encoded by nuclear genes.

The low-resolution form of the tetragonal crystal, with unit-cell parameters $a = b = 273.1$, $c = 170.9$ Å, was used for the structure determination. Molecular-replacement analysis was performed using the program *AMoRe* (Navaza, 1994) from the *CCP*4 suite (Collaborative Computational Project, Number 4, 1994).

Crystal structural analyses were monitored by evaluating the correlation coefficient $C = \sum(|F_o| - \langle|F_o|\rangle)(|F_c| - \langle|F_c|\rangle)/\sum[(|F_o| - \langle|F_o|\rangle)^2(|F_c| - \langle|F_c|\rangle)^2]^{1/2}$ and the R factor $R = \sum||F_o| - |F_c||/\sum|F_o|$. Abnormal overlapping among molecules in each crystal candidate structure was inspected to select an appropriate crystal structure.

3. Results

3.1. Crystal data

The intensity and crystal data of the hexagonal and the tetragonal crystals are given in Table 1. Another tetragonal crystal with unit-cell parameters $a = b = 253.2$, $c = 507.1$ Å diffracted X-rays to as high as 5 Å resolution and diffraction spots were systematically weak for $l = 3n + 1$ and $3n + 2$ reflections at low resolution. The specific intensity distribution indicates that the crystal structure has a pseudo one-third translation symmetry along the c axis of the unit cell. By soaking in such heavy-atom reagents as tetrakis(acetoxymercuri)methane, the crystal was transformed into a different phase of the same tetragonal system with unit-cell parameters $a = b = 273.1$, $c = 170.9$ Å, whose c axis was one-third that of

the original. The crystal diffracted X-rays at best to 15 Å and was isomorphous to the original crystal at low resolution judging from the intensity distribution. Thus, both tetragonal crystals were similar to each other in molecular packing.

3.2. Validity of crystal structures

Rigid-body refinement of the hexagonal crystal using a constrained monomeric structure in the asymmetric unit reduced the *R* factor to 0.314 at 9 Å resolution. The monomer in the asymmetric unit was transferred in one unit cell by crystallographic symmetry operations. Six monomers packed well without any molecular overlap in a unit cell of the crystal.

The low-resolution form of the tetragonal crystal with unit-cell parameters $a = b = 273.1$, $c = 170.9$ Å was used for the structural determination. Molecular-replacement analysis produced the first crystal structure candidate, with $C = 0.739$ and $R = 0.416$. The second candidate with $C = 0.676$ and $R = 0.451$, and the third candidate with $C = 0.653$ and $R = 0.482$ were rejected because of abnormal overlapping among 16 monomers in the unit cell. The first candidate showed reasonably satisfactory packing in the crystal. Both the criteria *C* and *R* for the first candidate deviate significantly from those of top 300 candidates, which had averaged values of 0.568 ($\pm$ 0.035) for *C* and 0.514 ($\pm$ 0.017) for *R*. Consequently, the first candidate appeared to represent the crystal structure of the tetragonal form. The crystal structure of the high-resolution form of the tetragonal crystal was not solved because of a problem with pseudo-translation symmetry.

3.3. Dimeric structures in hexagonal and tetragonal crystals

The crystal structures of the hexagonal and tetragonal crystals are schematically shown in Figs. 2(*a*) and 2(*b*), respectively. Two monomers around a crystallographic twofold axis at (1/2, 1/2, *z*) in the hexagonal crystal face each other to form a dimeric structure (Fig. 2*a*). A dimeric structure is formed around a crystallographic twofold axis at (1/4, *y*, 3/8) in the tetragonal unit cell (Fig. 2*b*). The orthorhombic crystal contains a dimer around a non-crystallographic twofold axis in the asymmetric unit, as shown in Fig. 3(*a*). Although the crystal structures of the hexagonal and the tetragonal forms were determined using the monomeric model of the orthorhombic form, dimeric structures appeared in the hexagonal and tetragonal crystals as shown in Figs. 3(*b*) and 3(*c*), respectively. The three dimeric structures in the hexagonal, tetragonal and orthorhombic crystals were compared by superposing one on another. Least-squares fittings for all the C^{α} atoms were executed among the three dimeric structures using the program *X-PLOR* (Brünger *et al.*, 1987). The r.m.s displacements were 0.30 Å between the dimers of the orthorhombic and hexagonal crystals, 0.98 Å between those of the orthorhombic and tetragonal crystals and 1.01 Å between those of the hexagonal and tetragonal crystals. The reason for the relatively high r.m.s. values against the tetragonal dimer is related to the low-resolution analysis at 15 Å. However, these r.m.s. values are low enough to conclude that assembly of the two monomers is identical irrespective of the crystal packing. This suggests that a characteristic property of the bovine heart cytochrome *c* oxidase is to form the dimeric structure. It should be noted that these low-resolution X-ray diffraction data provide significantly accurate information about the monomer–monomer assembly.

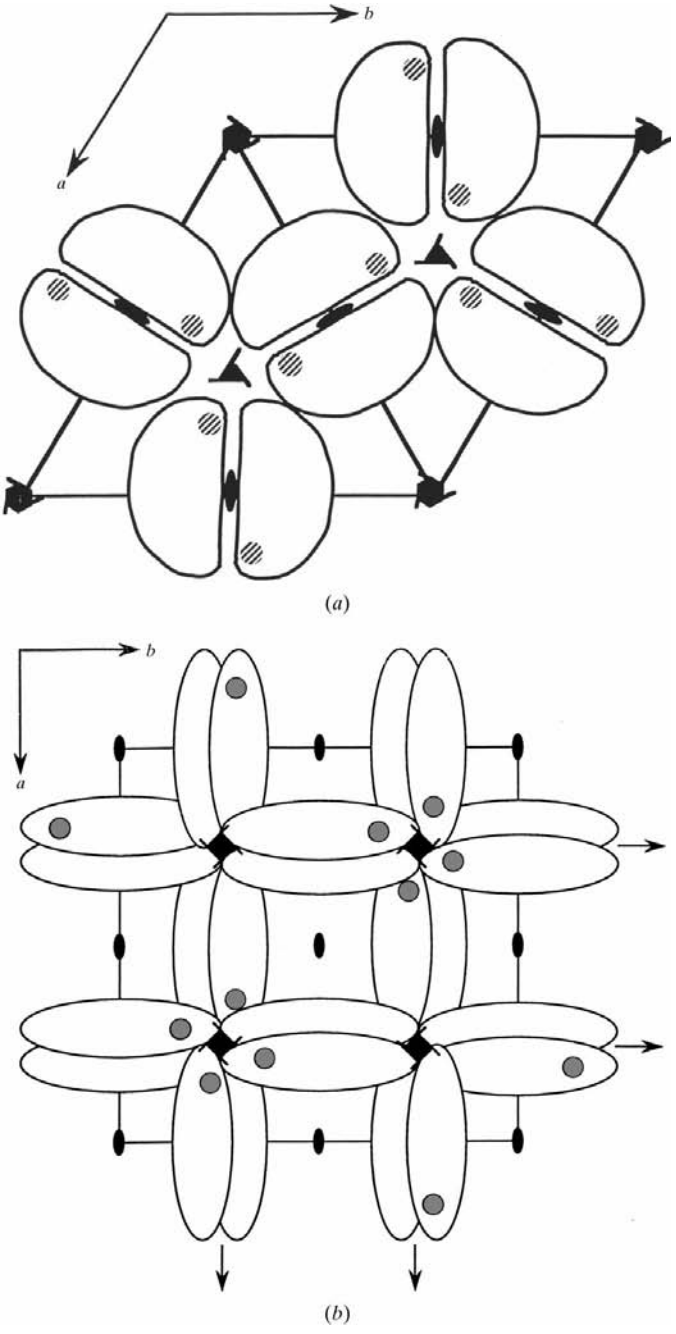

Figure 2
Schematic drawings of the crystal structures of bovine heart cytochrome *c* oxidase. (*a*) Molecules in the hexagonal unit cell are projected onto an *ab* plane. Each monomer, consisting of 13 different protein subunits, is represented by a half circle. A dimeric structure is identified at each crystallographic twofold axis. (*b*) Monomers, depicted by an oval shape in the tetragonal unit cell, are shown on an *ab* plane. Each asymmetric unit contains one monomer. Two monomers around a crystallographic twofold axis form a dimer.

3.4. Intermonomer interactions in a dimeric structure

Three regions for protein–protein interaction between monomers were identified by calculating intermonomer interatomic distances in the X-ray structure of the orthorhombic crystals. Lys46, Asp49, Ser51 and Val52 of subunit VIb of one monomer are in contact with Val52, Ser51, Asp49 and Lys46, respectively, of subunit VIb of the other monomer around a local twofold axis, as shown in yellow in Figs. 4(*a*) and 4(*b*). The second interaction is between subunits I and VIa of two different monomers and is shown in pink in Figs. 4(*a*) and 4(*b*). Subunit VIa exhibits a hook-shaped conformation at the N-terminal end. The ten N-terminal residues of subunit VIa extend into the transmembrane region and fit well into the cleft between helices V and VII of subunit I of the other monomer, as shown in Fig. 5. 14 residues of subunit VIa in the hook-shaped region, Ala1–Gly9, Arg14, Thr15, Phe18, Gly22 and Leu30, and 17 residues of subunit I, Ile169, Gln178, Tyr179, Met189, Ile190, Val193, Leu194, Leu197, Phe237, Met271, Trp275, Met278, Gly281, Phe282, Phe285, Ile286 and Ile311, are involved in the intermonomer hydrophobic interaction with interatomic distances of less than 4 Å. In addition to the hydrophobic interactions, two hydrogen bonds between subunits I and VIa, O^{η} (Tyr179 of subunit I)–$O^{\gamma1}$ (Thr15 of subunit VIa) and $N^{\varepsilon1}$ (Trp275 of

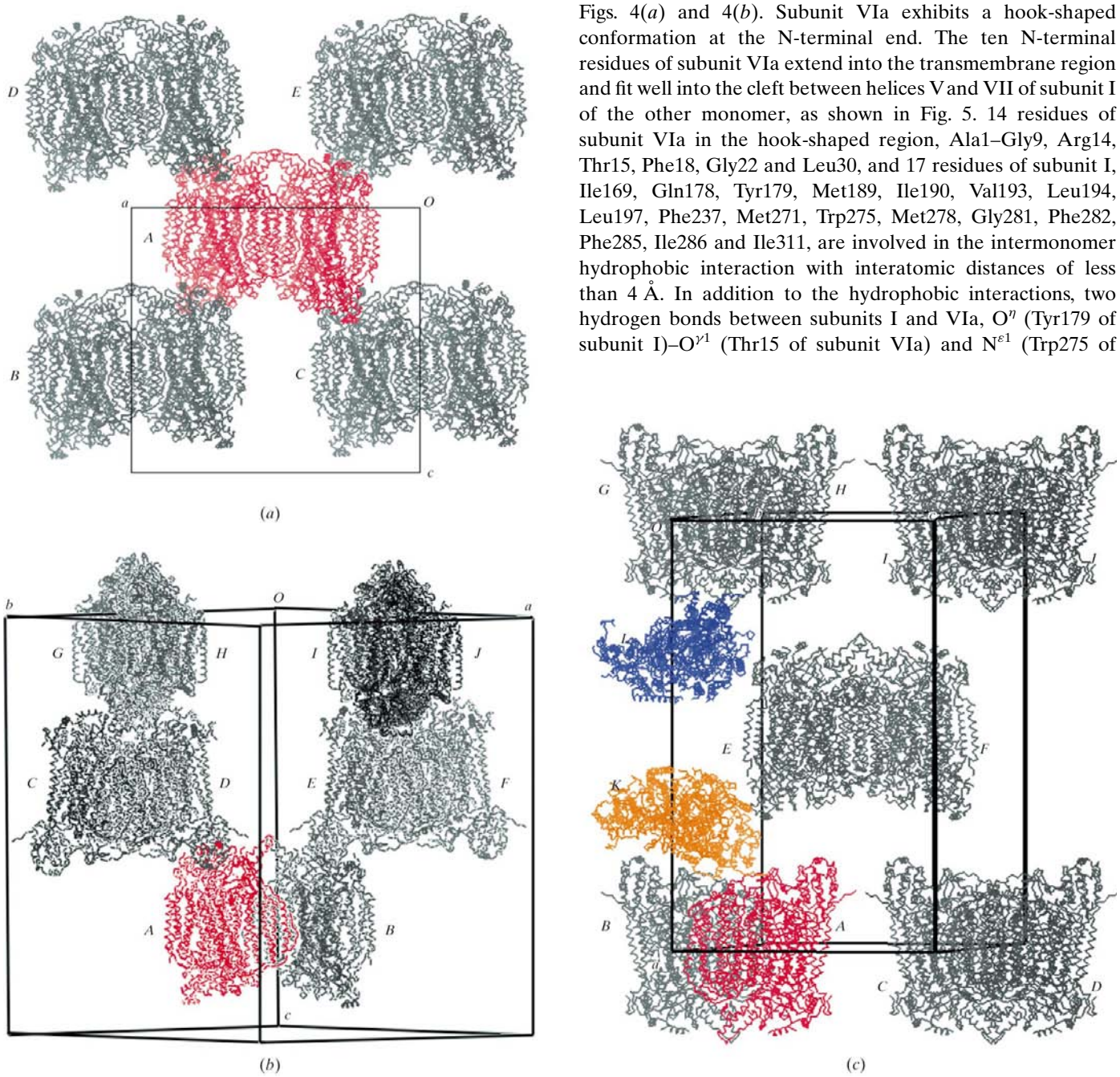

Figure 3
Dimeric structures of bovine heart cytochrome *c* oxidase obtained in three crystal forms are shown by C^{α} tracings. Each asymmetric unit is labelled by a capital letter representing a symmetry operation. Projected structures similar to those in an orthorhombic crystal are detected in both the hexagonal and tetragonal crystals. (*a*) Two monomers related by a local twofold axis nearly parallel to the *c* axis form a dimer in the orthorhombic crystal. An asymmetric unit contains a dimer coloured in red. Symmetry operations are as follows: *A*, (x, y, z); *B*, $(3/2 - x, -y, 1/2 + z)$; *C*, $(1/2 - x, 1/2 + y, 1/2 - z)$; *D*, $(3/2 - x, -y, -1/2 + z)$; *E*, $(1/2 - x, 1/2 + y, -1/2 - z)$. A dimer in an unit cell transferred by a symmetry operation of $(1 - x, 1/2 + y, 1/2 - z)$ is not shown to avoid confusion. (*b*) Molecules are shown in a hexagonal unit cell. Symmetry operations are as follows: *A* in red, (x, y, z); *B*, $(1 - x, 1 - y, z)$; *C*, $(y, y - x, -1/3 + z)$; *D*, $(1 - y, x - y, -1/3 + z)$; *E*, $(y, 1 + y, -1/3 + z)$; *F*, $(1 - y, 1 + x - y, -1/3 + z)$; *G*, $(1 + x - y, x, -2/3 + z)$; *H*, $(1 + y - x, 1 - x, -2/3 + z)$; *I*, $(x - y, x, -2/3 + z)$; *J*, $(y - x, 1 - x, -2/3 + z)$. (*c*) Molecules are shown in a tetragonal unit cell. Symmetry operations are as follows: *A* in red, (x, y, z); *B*, $(x, 1/2 - y, 1/4 - z)$; *C*, $(x, 1/2 - y, 5/4 - z)$; *D*, $(x, y, 1 + z)$; *E*, $(3/2 - x, y, 3/4 - z)$; *F*, $(3/2 - x, 1/2 - y, 1/2 + z)$; *G*, $(-1 + x, 1/2 - y, 1/4 - z)$; *H*, $(-1 + x, y, z)$; *I*, $(-1 + x, 1/2 - y, 5/4 - z)$; *J*, $(-1 + x, y, 1 + z)$; *K* in light brown, $(1/2 + y, 1 - x, 1/4 + z)$; *L* in blue, $(1/2 - y, -1 + x, -1/4 - z)$.

subunit I)–O (Gly22 of subunit VIa), contribute to stabilization of the dimeric structure. The side chains of Lys5, Asp7, His8 and Arg14 of subunit VIa are surrounded by polarized atoms such as carbonyl O atoms of subunit I. The third interaction between subunit Vb of one monomer and subunit Vb of the other monomer is shown in red in Figs. 4(*a*) and 4(*b*). The amino-terminal domain of subunit Vb of one monomer extends to the carboxyl-terminal domain of subunit Vb of the other monomer to make the close contacts Ala1–Glu64 and Ser2–Asp65 between the two monomers. The prominent interactions between subunits VIa and I are in the inner membrane region, while the interactions between subunits VIbs and between subunits Vbs are in the intermembrane and matrix spaces, respectively. The dimeric structure is strengthened to a high degree of stability by the wide range of intermolecular interactions.

3.5. Crystal packing and the quality of diffraction data

Crystal packing features of bovine cytochrome *c* oxidase are shown for three crystal forms in Fig. 6. Three crystals have interactions only in the hydrophilic part of the molecule. Of the three crystal forms, the orthorhombic crystal has the largest contact surface. In the orthorhombic crystal, the cytosolic site of one dimer makes contact with the matrix site of the other. One molecule of a dimer is related to the other by a local twofold axis parallel to the *c* axis. A total of 194 pairs of atomic contacts shorter than 4 Å were detected in interdimer interactions, subunit I–subunit IV, subunit II–subunit VIIc, subunit II–subunit VIII, subunit IV–subunit VIc, subunit Va–subunit VIc, subunit Vb–subunitVIIb, subunit VIc–subunit VIc, subunit VIc–subunitVIIc, subunit VIIa–subunitVIIb and subunit VIIb–subunitVIIc, in the crystal. Molecular interactions in the hexagonal crystal also occur along the *c* axis, but one dimer rotates about 120° against the other dimer. In this packing, the contact surface is significantly narrower than in the orthorhombic crystal. The major interaction is between subunit IV at the matrix site and subunit III at the cytosolic site. The crystal packing features of the tetragonal form are clearly different from both the above two crystals. As shown in Fig. 6, each tetragonal crystal has two interaction sites. These packing features are different from those of orthorhombic or hexagonal forms. The first site is between the cytosolic sites of subunit IV and subunit VIIb in one monomer of a dimer and the cytosolic sites of subunit IV and subunit VIIb in one monomer of another dimer. The second is between the matrix sites of subunit IV of one dimer and the matrix sites of subunit IV of another dimer.

4. Discussion

As stated above, the X-ray structures of the tetragonal and hexagonal crystals determined by the molecular-replacement method using the monomer model show dimeric structures identical to that of the orthorhombic crystals at 2.8 Å resolution. On the other hand, the dimer–dimer interaction is significantly different depending on the crystal packing. These two results indicate quite a strong interaction between the two monomers within the dimer.

The fairly hydrophilic N-terminal region of subunit VIa, including ten amino acids, is buried in the transmembrane region and three glycine residues are at the turning point in the hook-shaped conformation in the N-terminal region of subunit VIa. Thus, once the dimer is dissociated into two

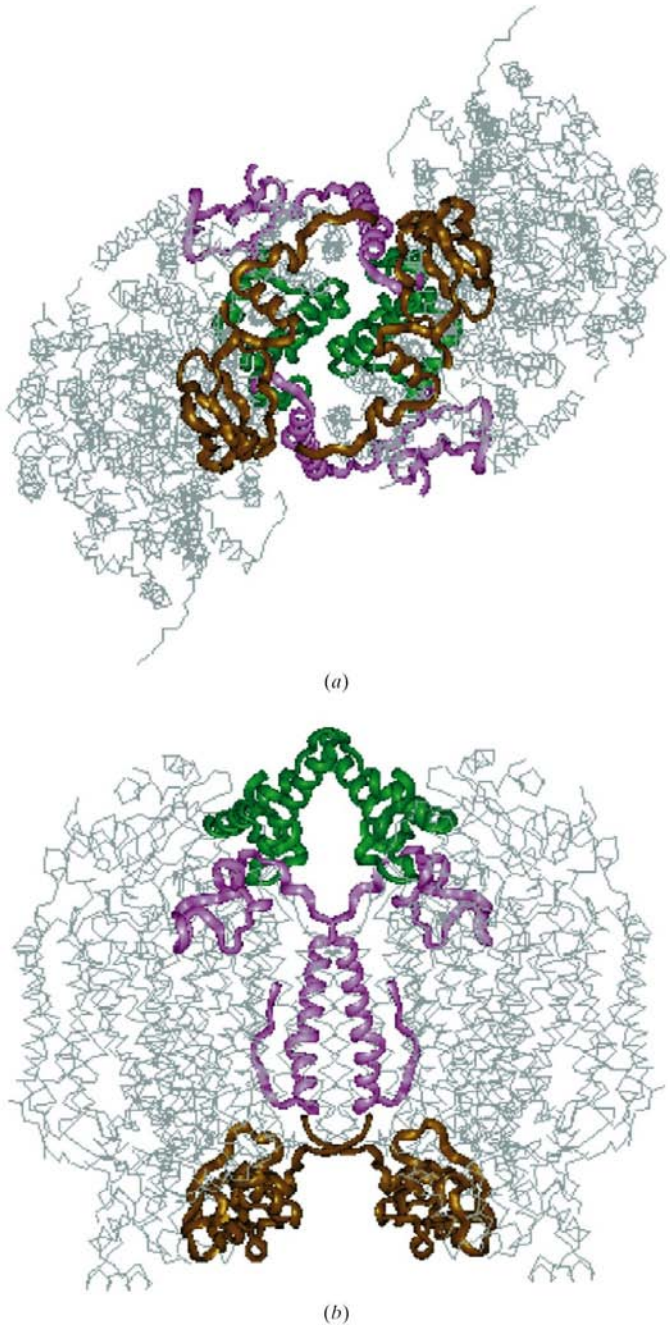

Figure 4
Monomer–monomer interaction in a dimeric structure. Subunits included in the intermonomer interaction are depicted by ribbon drawings. The subunits involved in intermonomer contacts are illustrated by ribbon models. The remaining subunits of the dimer are shown by wire models of C^{α} atoms. The yellow, pink and green structures denote subunits Vb, VIa and VIb, respectively. (*a*) Side view of the dimer. (*b*) Top view of the dimer from the matrix side.

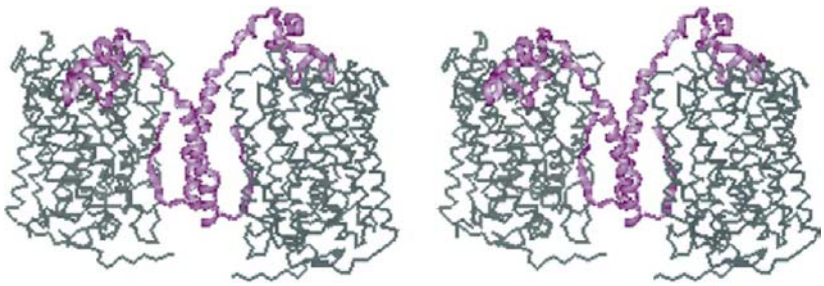

Figure 5
Stereo pair of subunits I and VIa in the dimer are illustrated by ribbon models of C^{α} atoms. Subunits I and VIa are shown in light and heavy lines, respectively.

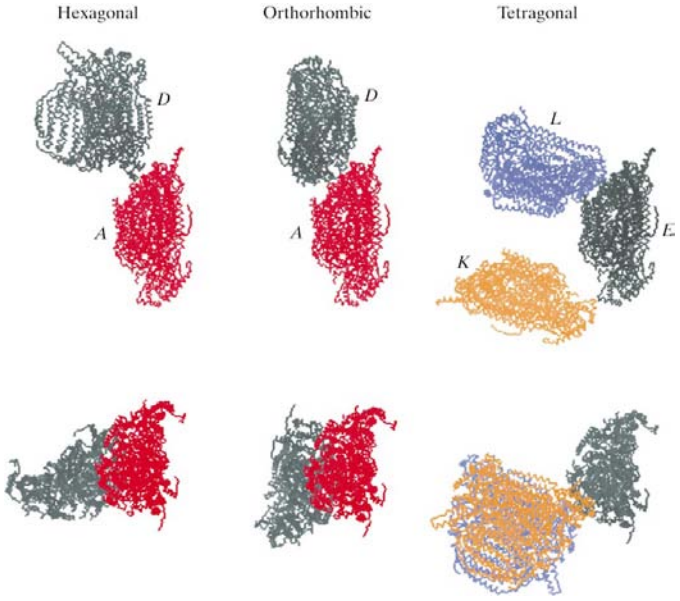

Figure 6
Intermonomer interactions of bovine cytochrome *c* oxidase are shown for three crystal forms. Top illustration in each crystal packing is a side view perpendicular to the *c* axis and the bottom illustration is a top view perpendicular to the *ab* plane. Capital letters for each crystal form represent the same symmetry operations as those given in Fig. 3.

monomers, the N-terminal region of subunit VIa will undergo a large conformational change resulting an extended conformation protruding into the matrix space. The hydrophilic nature of the N-terminal region would significantly inhibit the reverse conformational change from the extended conformation in the matrix space to the hook-shaped conformation in the hydrophobic transmembrane region. On the other hand, the conformation of the N-terminal region of subunit VIa, in addition to the two interactions in the extramembrane regions, strongly suggests that the intermonomer interactions are strong enough to prevent the dimer from spontaneous dissociation to two monomers. Thus, the dimeric state is likely to be dominant in mitochondrial membrane, although the possibility of the presence of the monomeric state cannot be excluded at present. The N-terminal portion of subunit VIa makes tight contacts with the surface of subunit I near the dioxygen-reduction site, suggesting that subunit VIa could control the function of the dioxygen-reduction site. On the other hand, Kadenbach's group proposed that a nucleotide binding to subunit VIa controls the efficiency of the proton-pumping function of this enzyme (Anthony *et al.*, 1993) and the nucleotide binding to subunit VIa has been confirmed by X-ray structure (Tsukihara *et al.*, 1996). These results suggest a regulatory function for subunit VIa in the dimeric state. The dimer formation observed in bovine heart cytochrome *c* oxidase is unlikely to occur in bacterial enzymes, which do not contain subunits corresponding to the nuclear-coded subunits (Iwata *et al.*, 1995).

This research was supported in part by Grants-in-Aid for 'Research for the Future' Program (JSPS-RFTF96L00503 to TT) from the Japan Society for the Promotion of Science, Grants-in-Aids for Scientific Research on Priority Area (10188101 and 10179101 to TT and 08249106 to SY) from the Ministry of Education and Culture of Japan and the Program for Promotion of Fundamental Studies in Health Sciences of the Organization for Pharmaceutical Safety and Research of Japan (to TT). TT and SY are visiting scientists of RIKEN.

References

Anthony, G., Reimann, A. & Kadenbach, B. (1993). *Proc. Natl Acad. Sci. USA*, **90**, 1652–1656.
Brünger, A. T., Kuriyan, J. & Karplus, M. (1987). *Science*, **235**, 458–460.
Capaldi, R. A. & Zhang, Y.-Z. (1986). *Methods Enzymol.* **126**, 22–31.
Collaborative Computational Project, Number 4 (1994). *Acta Cryst.* D**50**, 760–763.
Estey, L. A. & Prochaska, L. J. (1993). *Biochemistry*, **32**(48), 13270–13276.
Ferguson-Miller, S. & Babcock, G. T. (1996). *Chem. Rev.* **96**, 2889–2907.
Finel, M. & Wikström, M. (1986). *Biochim. Biophys. Acta*, **851**, 99–108.
Hakvoort, T. B., Moolenaar, K., Lankvelt, A. H., Sinjorgo, K. M., Dekker, H. L. & Muijsers, A. O. (1987). *Biochim. Biophys. Acta*, **894**, 347–354.
Hamilton, W. C., Rollett, J. S. & Sparks, R. A. (1965). *Acta Cryst.* **18**, 129–130.
Higashi, T. (1989). *J. Appl. Cryst.* **22**, 9–18.
Iwata, S., Ostermeier, C., Ludwig, B. & Michel, H. (1995). *Nature (London)*, **376**, 660–669.
Matthews, B. W. (1968). *J. Mol. Biol.* **33**, 491–497.
Navaza, J. (1994). *Acta Cryst.* A**50**, 157–163.
Rossmann, M. G. & Blow, D. M. (1962). *Acta Cryst.* **15**, 24–31.
Sakabe, N. (1983). *J. Appl. Cryst.* **16**, 542–547.
Shinzawa-Itoh, K., Ueda, H., Yoshikawa, S., Aoyama, H., Yamashita, E. & Tsukihara, T. (1995). *J. Mol. Biol.* **246**, 572–575.
Shinzawa-Itoh, K., Yamashita, H., Yoshikawa, S., Fukumoto, Y., Abe, T. & Tsukihara, T. (1992). *J. Mol. Biol.* **228**, 987–990.
Tomizaki, T., Yamashita, E., Yamaguchi, H., Aoyama, H., Tsukihara, T., Shinzawa-Itoh, K., Nakashima, R., Yaono, R. & Yoshikawa, S. (1999). *Acta Cryst.* D**55**, 31–45.

Tsukihara, T., Aoyama, H., Yamashita, E., Tomizaki, T., Yamaguchi, H., Shinzawa-Itoh, K., Nakashima, R., Yaono, R. & Yoshikawa, S. (1995). *Science*, **269**, 1069–1074.

Tsukihara, T., Aoyama, H., Yamashita, E., Tomizaki, T., Yamaguchi, H., Shinzawa-Itoh, K., Nakashima, R., Yaono, R. & Yoshikawa, S. (1996). *Science*, **272**, 1136–1144.

Yoshikawa, S., Shinzawa, K., Tsukihara, T., Abe, T. & Caughey, W. S. (1991). *J. Cryst. Growth*, **110**, 247–251.

Yoshikawa, S., Shinzawa-Itoh, K., Nakashima, R., Yaono, R., Yamashita, E., Inoue, N., Yao, M., Fei, M. J., Libeu, C. P., Mizushima, T., Yamaguchi, H., Tomizaki, T. & Tsukihara, T. (1998). *Science*, **280**, 1723–1729.

Yoshikawa, S., Shinzawa-Itoh, K., Ueda, H., Tsukihara, T., Fukumoto, Y., Kubota, T., Kawamoto, M., Fukuyama, K. & Matsubara, H. (1992). *J. Cryst. Growth*, **122**, 298–302.